JGR Solid Earth

RESEARCH ARTICLE
10.1029/2019JB017805

Collapse of Reacted Fracture Surface Decreases Permeability and Frictional Strength

K. Spokas[1], Y. Fang[2,3], J. P. Fitts[1], C. A. Peters[1], and D. Elsworth[2]

[1]Civil and Environmental Engineering Department, Princeton University, Princeton, NJ, USA, [2]Energy and Mineral Engineering, Pennsylvania State University, University Park, PA, USA, [3]Jackson School of Geosciences, Now at University of Texas at Austin, Austin, TX, USA

Key Points:
- Flow of acidic brine through fractures in mineralogically heterogeneous rocks selectively dissolves calcite and creates a porous layer
- Calcite-depleted porous layer collapses under normal stresses, filling the fracture with fine particles, decreasing permeability
- Layer of fine particles lowers fracture frictional strength because it prevents the formation of interlocking microasperities

Supporting Information:
- Supporting Information S1

Correspondence to:
C. A. Peters,
cap@princeton.edu

Citation:
Spokas, K., Fang, Y., Fitts, J. P., Peters, C. A., & Elsworth, D. (2019). Collapse of reacted fracture surface decreases permeability and frictional strength. *Journal of Geophysical Research: Solid Earth*, *124*. https://doi.org/10.1029/2019JB017805

Received 16 APR 2019
Accepted 4 DEC 2019
Accepted article online 7 Dec 2019

Abstract Geochemical and geomechanical perturbations of the subsurface caused by the injection of fluids present risks of leakage and seismicity. This study investigated how acidic fluid flow affects hydraulic and frictional properties of fractures using experiments with 3.8-cm-long specimens of Eagle Ford shale, a laminated shale with carbonate-rich strata. In low-pressure flow cells, one set of samples was exposed to acidic brine and another set was exposed to neutral brine. X-ray computed tomography and energy-dispersive X-ray spectroscopy revealed that samples exposed to acidic brine were calcite-depleted and had developed a porous altered layer, while the other set showed no evidence of alteration. After reaction, samples were compressed and sheared in a triaxial cell that supplied normal stress and differential pore pressure at prescribed sliding velocities, independently measuring friction and permeability. During the initial compression, the porous altered layer collapsed into fine particles that filled the fracture. This effectively impeded flow and sealed the fracture, resulting in fracture permeability to decrease 1 to 2 orders of magnitude relative to the unaltered fractures. This is a favorable outcome in subsurface applications where the goal is to reduce leakage risks. However, during shear the reacted fracture had lower frictional strength because the fine-grained particles in the collapsed layer prevented the formation of interlocking microasperities. Therefore, coupled geochemical and geomechanical processes that could favorably seal fractures could also increase the likelihood of induced seismicity. These findings have important implications for geological carbon sequestration, pressurized fluid energy storage, geothermal energy, and other subsurface technologies.

Plain Language Summary Underneath the surface of the earth lie many layers of rock formations. Some of these formations contain open pores where fluids can be stored. Natural examples include groundwater and oil formations. Many engineering applications utilize this space underground as storage. One example is the injection of greenhouse gasses for climate change mitigation. To prevent the fluids from leaking to the surface, storage rock formations are often located where overlying rock formation can contain fluids. Several risks include the inducement of small earthquakes and the leakage of fluids toward the surface. These risks are most prominent along rock fractures, where rock material is most susceptible to earthquakes and fluid can easily flow. In addition, the injection of fluids into the subsurface can produce acids that exacerbate these risks. In this study, we conducted experiments and found that these acids weaken fracture surfaces. Once exposed to mechanical stress, these surfaces collapse and seal the fracture. However, this collapse also decreases the frictional strength of the fracture. For relevant energy activities, these finding are helpful for minimizing the risks of injecting fluids underground. In context of climate change mitigation, these findings will help appropriate site selection to store greenhouse gas emissions safely.

1. Introduction

Subsurface energy activities often require the presence of impermeable caprock formations to reliably confine fluids. Examples include hydraulic fracturing, geologic carbon storage, compressed air storage, enhanced oil recovery, deep well disposal, and geothermal energy. However, the injection of fluids into subsurface reservoirs can produce geomechanical and geochemical perturbations that could compromise the integrity of the caprocks. Injection of fluids may result in the pressurization of subsurface fluids, the alteration of subsurface stresses, and the initiation of failure of preexisting fractures (Cornet et al., 1997; Ellsworth,

2013; Fang et al., 2016; Majer et al., 2007; Moeck et al., 2009; Rinaldi et al., 2015; Segall & Fitzgerald, 1998; Talwani, 1997; Walsh & Zoback, 2016; Zoback & Gorelick, 2012). Concurrently, the injection of fluids into the subsurface can create reactive fluids, such as the injection of CO_2 which dissolves in water and forms carbonic acid (Benson & Cole, 2008; Bielicki et al., 2018; Borgia et al., 2012; Gaus, 2010; Pearce & Dawson, 2018; Wilkins et al., 2016). Such reactive brines can enter and alter flow pathways by dissolving reactive minerals and increasing fracture permeability (e.g., Fitts & Peters, 2013; Hawkes et al., 2005). The interplay between these geomechanical and geochemical processes is still not fully understood and is the focus of this study.

Studies have shown that reactive flow can result in mineral dissolution that increases fracture permeability and exacerbates leakage risks. Laboratory and modeling studies have shown that many factors, such as flow rate, fluid reactivity, aperture distribution, and mineral heterogeneity, can significantly affect the pattern of mineral dissolution (Deng et al., 2015; Deng & Peters, 2019; Deng, Voltolini, et al., 2017; Deng et al., 2018; Elkhoury et al., 2013; Ellis et al., 2011; Polak et al., 2004; Spokas et al., 2018). In the context of carbon dioxide injection, injected fluid can dissolve into resident brines to form carbonic acid that can dissolve rock material and enlarge fractures. One mineral highly susceptible to dissolution is calcite. Given calcite's high thermodynamic solubility, fast kinetics, and abundance in subsurface rock formations, calcite-rich rock formations are considered to be the most susceptible to porosity and porosity-driven permeability increases (Fitts & Peters, 2013). For mineralogically heterogenous fractures that contain minerals with different reactivities, reactive flow can deteriorate fracture surfaces by preferentially dissolving fast-reacting minerals. This can create “altered” or “degraded” layers of high porosity and low preconsolidation strength at the surface (Ajo-Franklin et al., 2018; Akrad et al., 2011; Dávila et al., 2016; Deng et al., 2013; Deng et al., 2016; Elkhoury et al., 2013; Ellis et al., 2011; Ellis & Peters, 2016; Rohmer et al., 2017). While it is clear that reactive flow can lead to changes both in mineralogy and roughness at the fracture surface, the effects of reaction on geomechanical and hydrodynamic behavior remain unclear.

The geomechanical stability of fractures or faults is governed by their frictional properties, which can be summarized by two main parameters, the frictional strength μ and the frictional stability (a-b) value (Dieterich, 1978; Ruina, 1983). The former governs the magnitude of shear stress necessary to induce failure and the latter describes how the fracture shear failure will behave. Two possible shear failure behaviors are velocity-strengthening and velocity-weakening. Velocity strengthening behavior results in aseismic (stable) slip while velocity-weakening behavior is a necessary condition for seismic (unstable) slip. In general, experimental observations have shown that frictional strength and stability follow a reverse relationship: when strength is high, stability is low, as summarized in Fang, Elsworth, Wang, et al. (2018). Microphysical models have shown that this results from the mechanics of surface contact and microstructure deformation of individual crystalline phases (Niemeijer & Collettini, 2013; Niemeijer & Spiers, 2007). In addition, many nonmineralogical factors, such as temperature, normal stress, pore fluid pressure, displacement, and velocity, also influence strength and stability (Rohmer et al., 2016).

The mechanical properties of crystalline phases, such as plasticity, brittleness, ductility (Fang et al., 2017; Fang, Elsworth, Wang, et al., 2018; Ikari et al., 2011; Kohli & Zoback, 2013; Niemeijer & Collettini, 2013), and swelling characteristics (Fang et al., 2017; Heiduc & Wong, 1996, Xu & Pruess, 2004), ultimately influence the deformation of rock material at the fracture surfaces during shear. Experiments have shown that the presence of swelling phyllosilicate phases often result in fractures that have lower frictional strength, higher frictional stability, and greater permeability reduction when sheared in the presence of brine (Bourg, 2015; Fang et al., 2017; Fang, Elsworth, Wang, et al., 2018; Norrish & Quirk, 1954). Conversely, fractures with nonswelling and hard mineral phases, such as tectosilicates or carbonates, often exhibit high frictional strength but result in dilation during shear that results in permeability increases (Fang et al., 2017; Fang, Elsworth, Wang, et al., 2018; Guglielmi et al., 2015; Wang et al., 2017).

In addition to mineralogy, surface roughness of the rock fracture has also been shown to affect the frictional and permeability behavior during shear. Increased fracture surface roughness can result in higher frictional strength and stability, resulting from an increase in the number of cohesive interlocking asperities (Fang, Elsworth, Ishibashi, et al., 2018). These asperities result in alternating periods of fracture compaction and dilation during shear, leading to permeability fluctuating more than in smooth fractures. Therefore, both the mineralogical compositions and surface roughness of a rock fracture affect whether a fracture

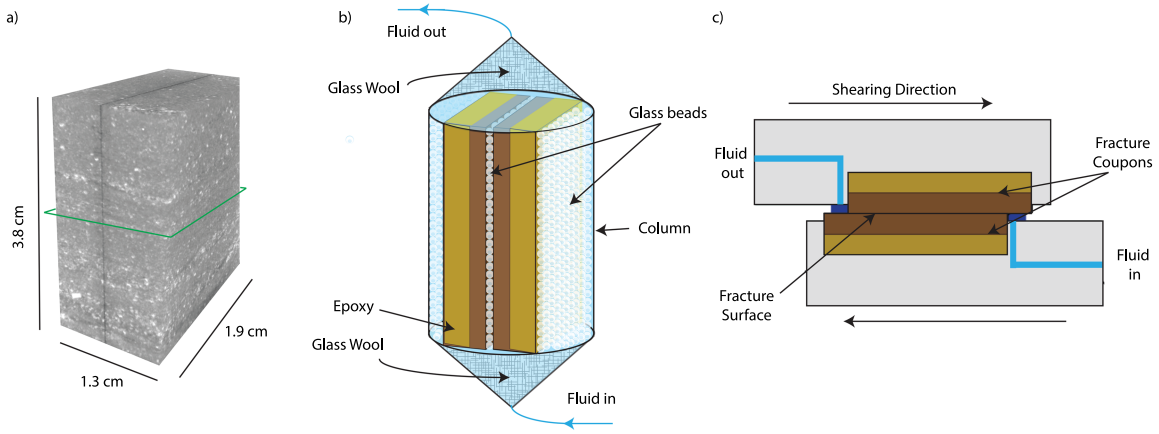

Figure 1. (a) Three-dimensional XCT image of paired rock coupons. Green rectangle indicates the orientation of the cross sections of the XCT images. (b) Paired rock coupons in the low-pressure flow cell. (c) Rock coupons sheared in experimental apparatus (modified from Fang, Elsworth, Wang, et al. (2018); see supporting information).

experiences shear-induced dilation or compaction (Niemeijer & Collettini, 2013; Niemeijer & Spiers, 2007), which ultimately influences the permeability response of the fracture to shear.

Given that the frictional and permeability behavior of fractures during shear is linked to mineralogy and surface roughness, it can be hypothesized that the flow of reactive fluid that alters both mineralogy and surface roughness will affect the frictional behavior of fractures. To date, few data exist on the effect of mineral reactions on the frictional properties of fractures. Samuelson & Spiers (2012) reported no clear influence of reactive brine exposure on clay- and quartz-rich gouge frictional properties. However, the samples in that study contained no fast-reacting minerals, such as calcite. Alternatively, Pluymakers et al. (2014) reported decreases in frictional strength for anhydrite gouge exposed to CO_2 and water, while Fang, Elsworth, Wang, et al. (2018) reported that carbonate crystalline phases at the fracture surface increase frictional strength and stability. In addition, it is not well understood how mineral-depleted surfaces behave during shear or how such surfaces affect the fracture frictional behavior during shear. To ultimately assess the severity of the risk of injecting fluid that can acidify resident brines and change the integrity of caprocks, understanding the coupling between geochemical and geomechanical processes is necessary.

The primary objectives of this paper are to produce deteriorated fracture surfaces that result from selective mineral dissolution under acid conditions and to explore the effect of these reacted fracture surfaces on fracture friction and permeability during shear. One hypothesis could be that the reacted surfaces will lead to a decrease in fracture strength and stability. However, an alternate hypothesis could be that reacted surfaces will increase fracture surface roughness, which has been shown to increase frictional strength (Fang, Elsworth, Ishibashi, et al., 2018). In this study, we used 3.8-cm-long samples of Eagle Ford shale (Figure 1a), a stratified shale that has carbonate-rich strata. This is representative of a rock that could be used as a caprock formation to seal the injection of fluids, such as carbon dioxide, and is susceptible to carbonate dissolution during reactive flow. To investigate this objective, this study presents a two-part experiment involving (1) low-pressure reactive flow experiments (Figure 1b) and (2) velocity stepping shearing experiments (Figure 1c) with imaging occurring at multiple stages. This work combines an array of analytical methods, including X-ray computed tomography (XCT) for 3-D imaging, X-ray diffraction (XRD) for mineral identification, bulk energy-dispersive X-ray fluorescence spectroscopy (ED-XRF) for element mapping, and scanning electron microscopy augmented with energy-dispersive X-ray spectroscopy (SEM-EDS) for mineral identification and localization.

2. Experimental Methods

2.1. Sample Materials

Samples of Eagle Ford shale, originally taken from an outcrop, were purchased from Kokurec Industries. The Eagle Ford shale is an organic-rich laminate shale in southern Texas that is actively drilled for

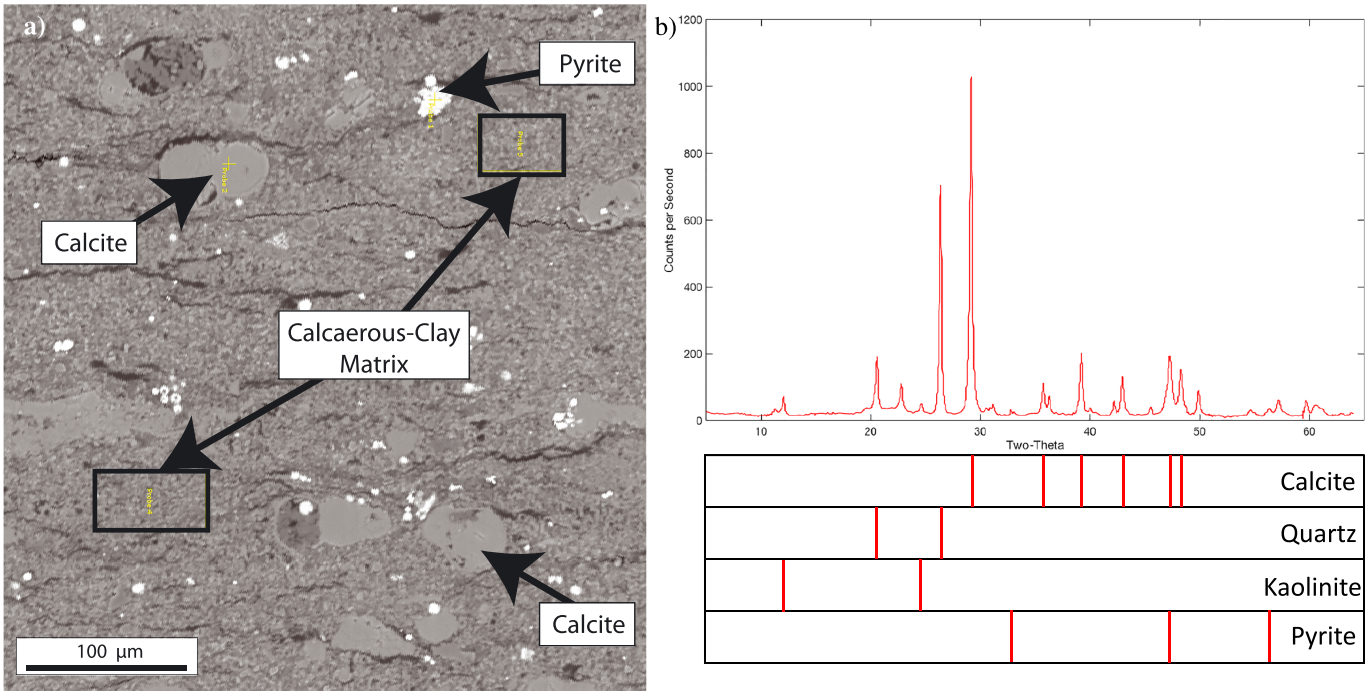

Figure 2. (a) SEM image of Eagle Ford shale with identified pyrite, calcite grains, and fine grained calcareous-silicate matrix. Small yellow markings show SEM-EDS probe locations. (b) XRD analysis of homogenized sample.

unconventional oil and gas operations. Rectangular samples were cut with the long dimension perpendicular to the sedimentary bedding planes, resulting in eight paired coupons measuring 1.3 × 3.8 × 1.9 cm (Figure 1a). Fracture surfaces were roughened using a 60-grit abrasive.

Mineralogical composition was analyzed by Applied Petrographic Services using XRD, ED-XRF, and SEM-EDS. The Eagle Ford shale samples in this study are calcareous mudstone consisting of ultrafine-grained calcite and silicate minerals arranged in a foliated texture with concentrated layers of larger calcite grains (Figure 2). Powder XRD analysis identified the carbonate as calcite. Silicate minerals include quartz and kaolinite, and trace amounts of pyrite are also present throughout the sample. Bulk oxide compositions determined by ED-XRF show 30.1 and 32.3 wt % of CaO and SiO_2 in the original sample, respectively (supporting information).

2.2. XCT

Samples were imaged by XCT before and after each stage of the experiment to observe the structure of the reaction-altered fracture surface and the new void space caused by mineral dissolution. Scanning was conducted at the Princeton University Imaging and Analysis Center with a ZEISS Xradia 520 Versa X-ray microscope at 110 keV, 83.5 μA, using a 0.4X magnification lens, resulting in a 3-D image with a voxel size of ~10 μm. This imaging enabled visual examination of fracture surfaces at each stage of the experiment, which is important for distinguishing physical differences between sample sets after flow and shear.

2.3. Reactive Flow Experiments

Reactive flow experiments were done to expose the fractures to acidic and neutral brines (Figure 1b). The surfaces on the outsides of the coupons were coated with epoxy to prevent through-flow and reaction. One set of rock coupons was exposed to 1 mol/L NaCl brine that was acidified to pH 2.5 by the addition of hydrochloric acid. This pH can be compared with a pH of 3 that may occur from carbonic acid in nonalkaline saline water in contact with pressurized CO_2 at a depth of ~1 km (Ellis et al., 2010). The choice of using hydrochloric acid allows for investigation of the dominant acid-driven mineral dissolution with controlled pH and eliminates the need to control gas-phase pressure, a significant practical limitation. A second set of samples was exposed to a neutral 1 mol/L NaCl brine that was created by adding sodium bicarbonate

to achieve pH of 7.8. In a given flow experiment, two sample coupons were inserted into a cylindrical flow column and separated by glass beads along the fracture surface and glass wool was used at the inlet and outlet (Figure 1b). The glass beads dispersed the influent across the entire surface of the coupons promoting uniform alteration of the reacted fracture surface. This was intended to prevent localized reacted and unreacted zones and avoid fracture surface channelization which would complicate interpretation of the experiments. Fluid flow rate was set constant at 1 mL/min with an ISCO 500D pump for a total flow volume of 10 L over the course of seven days.

2.4. Shear Experiments

After reactive flow, for each of the eight paired coupons the glass beads were removed from between the coupons and the pieces were put back together to form a representation of a fracture. The samples were compressed and sheared under confining stress using an experimental apparatus at Pennsylvania State University (Figure 1c). We utilized experimental methods described in Fang, Elsworth, Wang, et al. (2018). The triaxial testing apparatus is capable of independently setting shear velocity, confining stress, and upstream fluid pressures, and measuring shear stress and fluid flow rate using three independent ISCO 500D pumps. Downstream pore pressure is ambient pressure. Lastly, shear displacements are measured using a linear variable differential transformer.

For the experiments, the confining stress and pore fluid pressure were set to create a constant effective normal stress of 3.2 MPa. Effluent flow rate was measured during the initial increase of confining pressure prior to shear and during shear. To avoid the flow of brine around the sample and to ensure flow through the fracture, flow was initiated after the confining pressure had reached 250 kPa. Permeability measurements were reliable for four of the samples. Shear velocity was incrementally increased and decreased between 1 and 10 μm/s until a maximum displacement of ~6 mm was reached (supporting information).

The coefficient of friction, also known as frictional strength μ, was determined using the ratio of shear stress τ (Pa) to applied effective normal stress σ'_n (Pa; ignoring the cohesive strength) as

$$\mu = \tau/\sigma'_n \tag{1}$$

The value of frictional stability $(a - b)$ in response to a change in velocity, V (μm/s), was determined by the empirical rate-and-state friction theory (Dieterich, 1978; Dieterich, 1979; Fang, Elsworth, Wang, et al., 2018; Marone, 1997; Ruina, 1983; Scholz, 1998) as

$$(a-b) = \frac{\Delta\mu_{ss}}{\Delta lnV} \tag{2}$$

where a and b are the frictional constitutive parameters, which represent the effects of instantaneous and displacement-dependent changes in friction, respectively, and $\Delta\mu_{ss}$ is the change in the coefficient of friction. Fractures with positive $(a - b)$ values show velocity-strengthening behavior while negative $(a - b)$ values show velocity-weakening behavior.

Permeability, $k(m^2)$, was evaluated assuming the cubic law of a single fracture (Witherspoon et al., 1980; Fang, Elsworth, Wang, et al., 2018; Ishibashi et al., 2018), and using the measured fluid flow rate for a given pressure differential:

$$b = -\left(\frac{12\mu \cdot L(t) \cdot Q(t)}{W \cdot \Delta P}\right)^{\frac{1}{3}} \tag{3}$$

$$k = \frac{b^2}{12} \tag{4}$$

where μ (Pa·s) is the viscosity of the fluid, $L(t)$ (m) is the contact length of the fracture surface, W (m) is the fracture width, $Q(t)$ (m^3/s) is the measured flow rate, and ΔP (Pa) is the differential pressure between the upstream and downstream limits of the fracture.

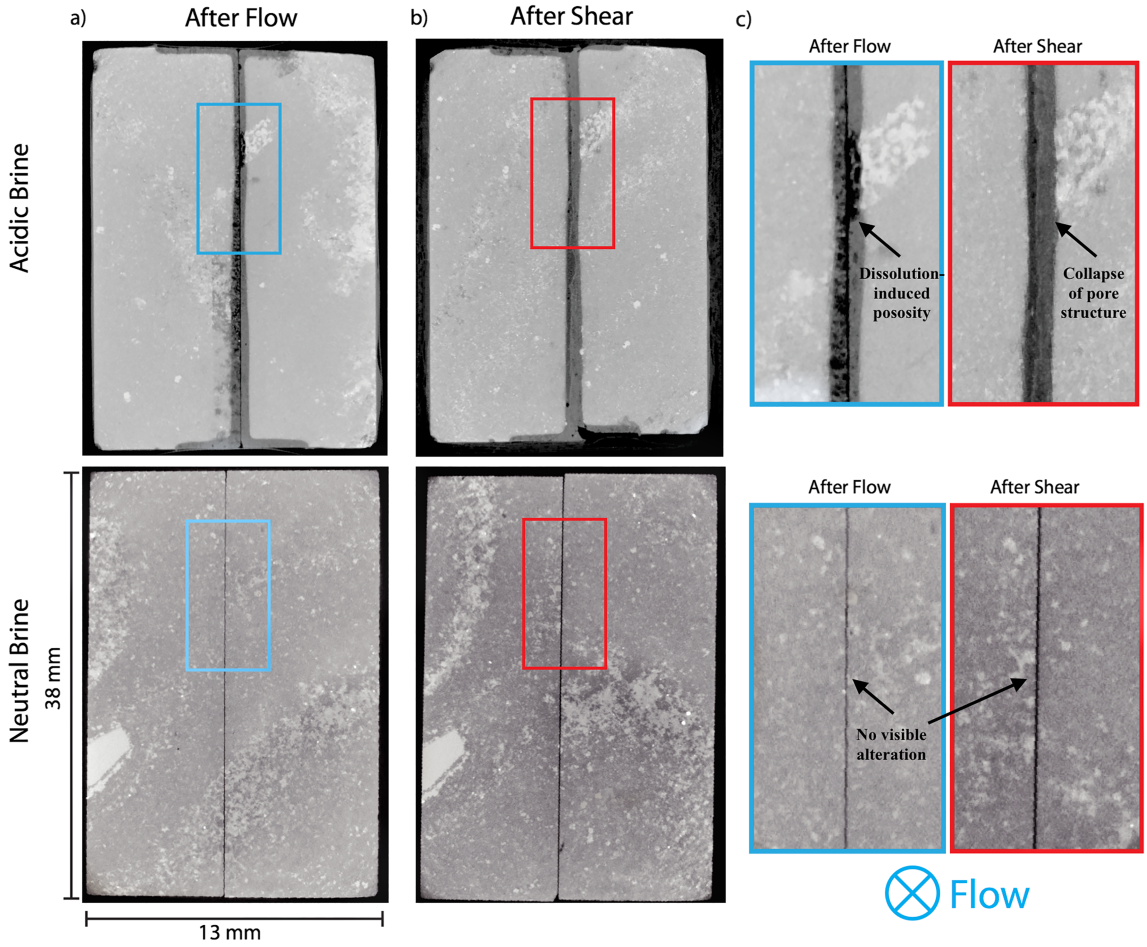

Figure 3. Cross sections from the XCT 3-D images of the rock coupon pairs: (a) after flow, (b) after shear, and (c) magnification of the fracture surface for the acidic (above) and neutral (below) experiments.

3. Results and Discussion

3.1. Reactive Flow Results

XCT imaging reveals the resulting physical alteration of the fracture surfaces caused by flow in comparison to images scanned before the flow experiment (Figure 3). Samples exposed to the acidic brine show significant alteration to a depth of approximately 0.75 mm from the fracture into the rock matrix, with new void space having been created where calcite grains had been present (Figure 3b). In the XCT image, the remaining rock material in the altered layer appears darkened, indicating the creation of void space.

One altered sample was epoxied and thin-sectioned for SEM-BSE analysis and SEM-EDS analysis. Figures 4a and 4b provide two SEM-BSE images of the reaction front boundary at different magnifications. SEM-EDS spectra of the altered and unaltered zones in a sample exposed to the acidic brine reveal that the difference in composition is dominated by the removal of calcium in the altered zone. Given that powder XRD analysis had revealed calcite to be the only calcium-bearing mineral, the depletion in calcium is due to calcite mineral dissolution. Location 2 provides an example of a coarse calcite grain undergoing dissolution at the reaction front. It is possible that some of the silicate minerals dissolved, including kaolinite, but the thermodynamics of those reactions and their kinetics are far less favorable than calcite dissolution (Fitts & Peters, 2013). Dissolution of the distinct calcite grains results in the formation of void spaces as large as ~100 μm. Location 3 provides an example of a calcite grain that undergoes transport-limited dissolution due to its surrounding rock material, making the calcite grain remain in the altered layer. In addition to coarse grain dissolution, areas containing finely grained calcite in the matrix results in microscale voids in

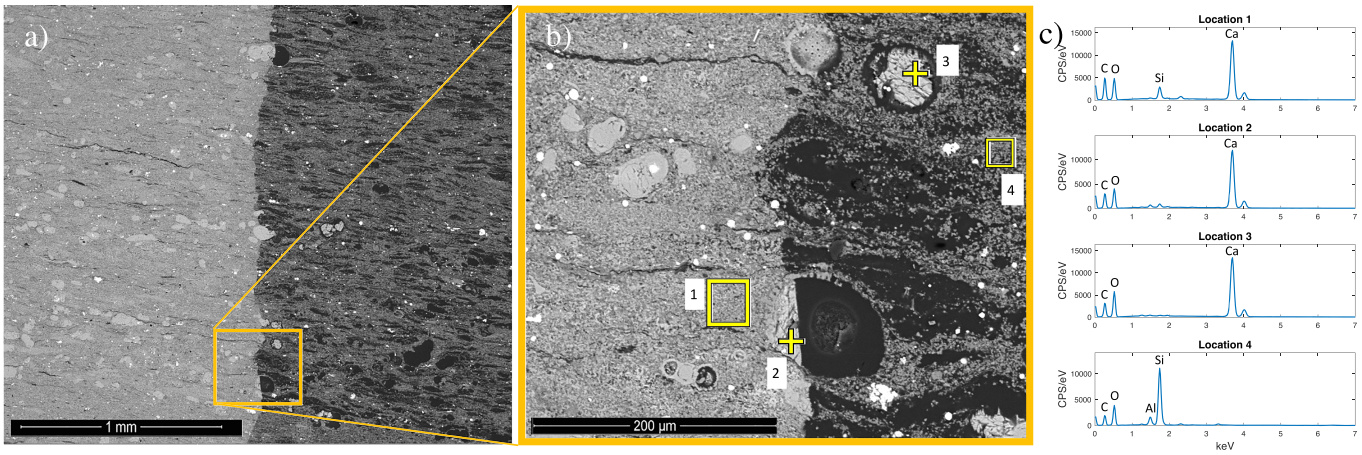

Figure 4. (a and b) SEM-BSE images of the reaction front after exposure to acidic fluid with (c) EDS spectra of four locations near the front.

the remaining altered layer material (e.g., Location 1 versus Location 4). Location 4 is depleted in calcium, leaving behind a fine-grained porous quartz- and kaolinite-rich matrix.

This type of dissolution-induced porous layer can be described as an "altered layer" (Deng et al., 2016), "degraded zone" (Ellis et al., 2011), or "microporous phase" (Noiriel et al., 2007) and is bounded by the dissolution region (Elkhoury et al., 2013; Noiriel et al., 2007). This sharp and even reaction front reflects the diffusion-limited reaction front propagation in a relatively homogenous rock material at this spatial scale. The formation of porosity at the fracture surface has implications for the preconsolidation strength, which determines the maximum stress that the surface can endure without collapsing. Porosity is inversely related to the preconsolidation stress of rock material and has been shown to decrease due to the creation of dissolution-induced porosity (Rohmer et al., 2017). The lower the preconsolidation strength is, the more susceptible the material is to collapse under normal stress. Therefore, although it was not measured directly, it can be postulated that the creation of porosity for the samples exposed to acidic fluid likely decreased the preconsolidation strength of the fracture surface and made this layer susceptible to collapse. This will be further addressed in section 3.2.

Samples exposed to neutral brine show no chemical alteration, with calcite grains persisting at the fracture surface (Figure 3c).

3.2. Permeability

The permeability measurements during the initial ramp-up in confining pressure and during shear for four samples, two from each pH condition, are shown in Figure 5. Between 250 and 3,000 kPa, measurements show that the permeability of the two acid-reacted samples decreased 1 to 2 orders of magnitude compared to the two samples exposed to the neutral brine, which remained relatively constant (Figure 5a). It is postulated that the porous layer of the acid-reacted samples likely collapsed during the initial ramp-up in confining pressure. This is supported by the XCT image in Figure 3e, which shows that after shearing the porous altered layer has been comminuted and become a layer of fine-grained rock material. This layer of fine particles fills much of the aperture between the two rock coupons with particles. Gaps observed in Figure 3e are caused by postexperiment sample handling that required the two fracture halves to be separated and put back together. From one altered and sheared sample, the layer of fine-grained rock material was sampled by scraping material into a deionized water and acetone solution. Droplets of the fine-grained rock solution were dried on silicon platelets and analyzed using SEM-EDS (Figure 6). Particle sizes ranged from ~1 to 100 µm, with the fine-grained particles made up dominantly of quartz with traces of titanium oxide (Figure 6a) and increasing in chemical complexity for larger aggregated particles (Figure 6c).

Therefore, we hypothesize that the 1 to 2 orders of magnitude decrease in permeability is the result of the altered porous layer collapsing during the initial compression of the sample and filling the fracture void space with fine-grained altered rock material. This is analogous to permeability reductions caused by the

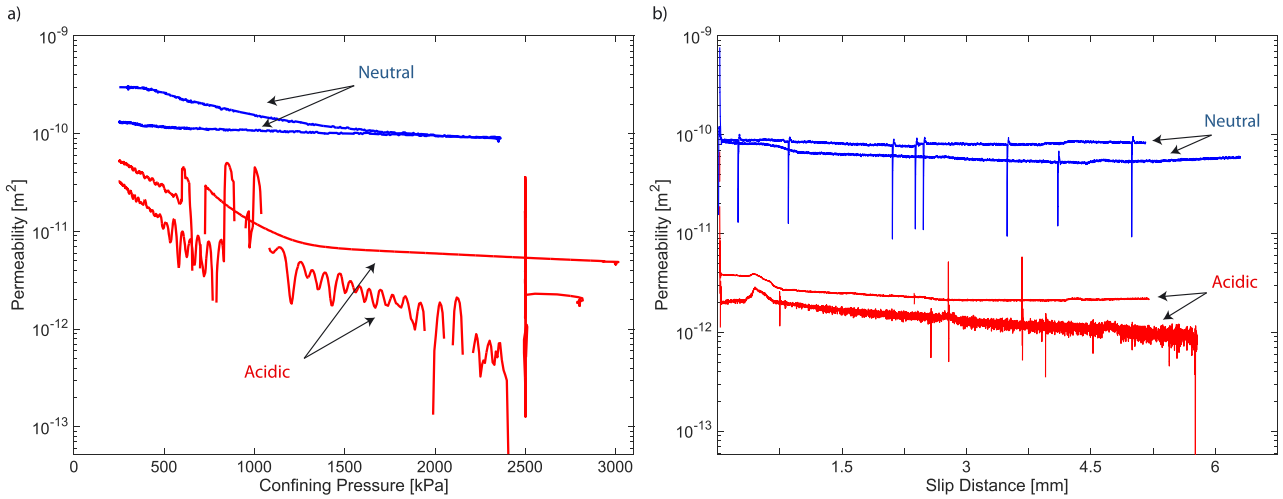

Figure 5. (a) Permeability evolution during the initial increase in confining pressure and (b) permeability during the shearing experiment of four samples, two exposed to acidic brine and two exposed to neutral brine.

formation of wear products and gouge during shear (Faoro et al., 2009). The difference in permeability between the neutral and acid-reacted fractures persisted during the entire shearing experiment (Figure 5b). This suggests that the deformation that occurred during the initial compression of the samples is significant and dominated the evolution of permeability during the entire experiment. While deformation during shear likely further ground the particles between the fracture walls, it does not appear to have significantly further reduced the permeability in either sample set.

3.3. Friction and Permeability Behavior During Shear

Frictional strength and stability measurements taken during velocity up-steps for the eight samples, four from each set of pH conditions, are shown in Figure 7. Each shearing experiment included two velocity up-steps (supporting information); the measurements from the first and second up-steps are represented

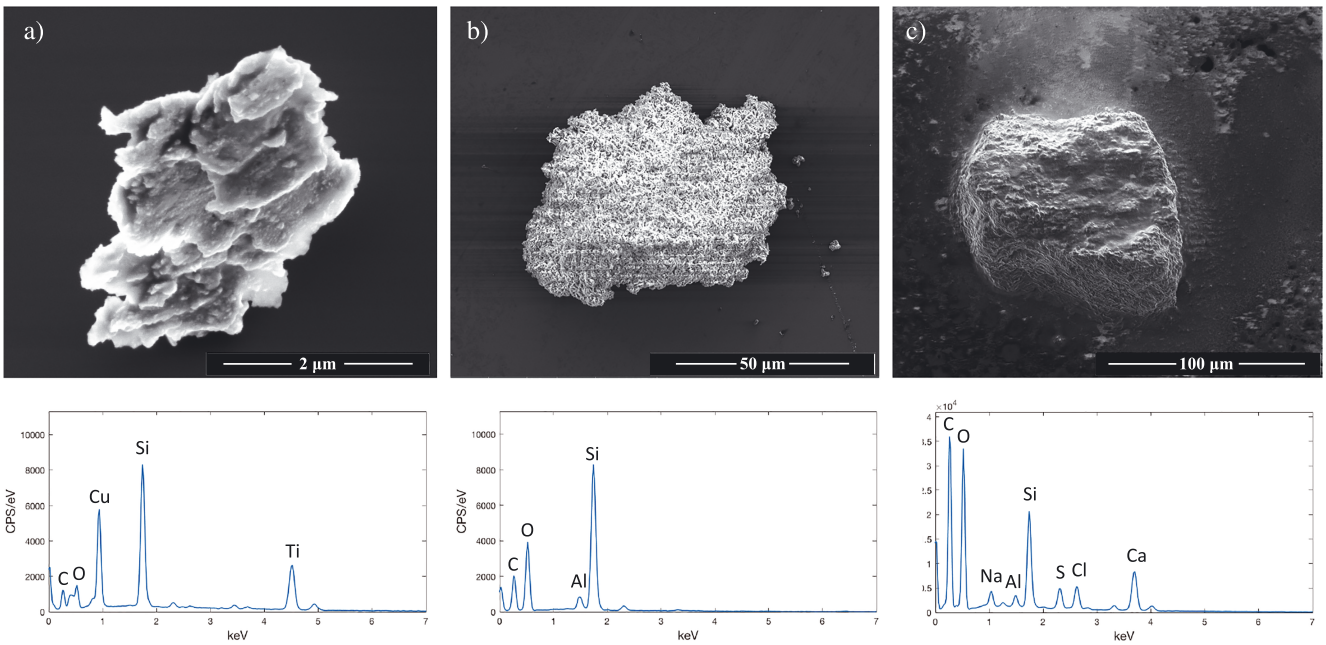

Figure 6. (top) SEM imaging and (bottom) SEM-EDS spectra of (a–c) three fine-grained particles from the collapsed altered layer.

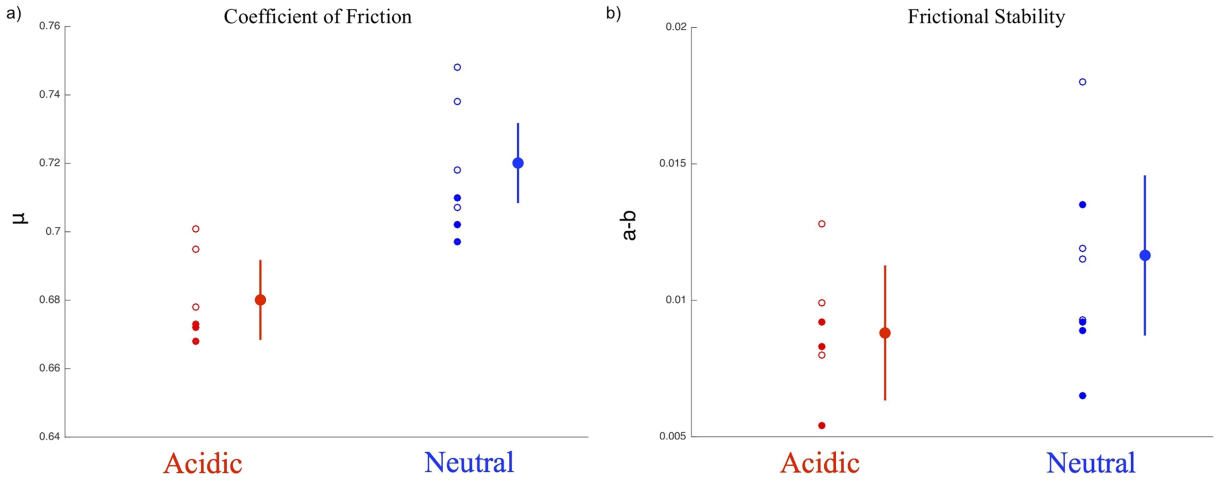

Figure 7. (a) Coefficient of friction and (b) frictional stability after first (full circle) and second (hollow circle) velocity up-steps. Means and 95% confidence intervals are shown with circles and bars to the right of the data.

by solid and hollow circles, respectively. Comparison between the acid-reacted and neutral samples shows that the acid-reacted samples exhibited lower frictional strength. The difference between the frictional strength of the sample sets is statistically significant at the confidence interval of 95%. The means and the 95% confidence intervals for the two samples sets are 0.68 ± 0.013 for the acid-reacted experiment and 0.72 ± 0.015 for the neutral flow experiment. The statistically significant difference between the frictional strengths of the sample sets provides evidence that dissolution-induced alteration reduces fracture frictional strength. For the frictional stability measurements, there appears to be a slight trend that the acid-reacted samples have lower stability, but the 95% confidence intervals significantly overlap and fail to exhibit a statistically significant difference.

This result is explained by two factors that sequentially changed the fracture surface: (1) mineral dissolution of calcite and the (2) collapse of the porous altered layer. For the first factor, the flow of reactive fluid dissolved and removed calcite asperities from the fracture surface. Previous observations have illustrated that increasing calcite content often corresponds to greater frictional strength and stability due to the strong and brittle structure of calcite (Fang, Elsworth, Wang, et al., 2018). Therefore, the reduction of frictional strength due to the removal of calcite in this study agrees with previous experimental findings. For frictional stability, the results presented here also agree with previous experimental findings that show weak to no correlation between carbonate content and stability (Fang, Elsworth, Wang, et al., 2018). For the second factor, the eventual collapse of the fracture surface exposed to acidic brine significantly altered the structure of the fracture surface compared to the samples exposed to neutral brine. Effectively, the collapse created a layer of fine particles between the two fracture walls that acted as a slipping plane.

An interpretation of the coupling between flow, geochemistry, and geomechanics throughout the stages of the experiment is schematically shown in Figure 8. The stages and mechanisms depicted in Figure 8 are inferred from the previous XCT, SEM-BSE, SEM-EDS, and XRD observations. For both experiments, the original fractures had microroughness present on the fracture surfaces (Figure 8b). For the samples exposed to acidic brine, dissolution of calcite created new void spaces, removed calcite-cement in the rock matrix, and ultimately decreased the preconsolidation strength of the fracture surface (Figure 8c). For samples exposed to neutral brine, no chemical alteration occurred (Figure 8d). During initial compression of the samples in the shearing apparatus, the altered surfaces of the acid-reacted samples collapsed and filled the fracture with fine particles. This prevented the formation of microasperities and effectively created a slipping plane (Figure 8e). This is consistent with weak faults, often clay-rich, where large amounts of gouge can be found (Ikari et al., 2009). For the control samples, initial compression of the two fracture surfaces resulted in the microroughness interlocking to become microasperities (Figure 8f), which ultimately increased the frictional strength of this sample set relative to the other. Lastly, the acid-reacted samples effectively "surfed" on the layer of fine particles during shear, as particles grinded and displaced inside the layer (Figure 8g).

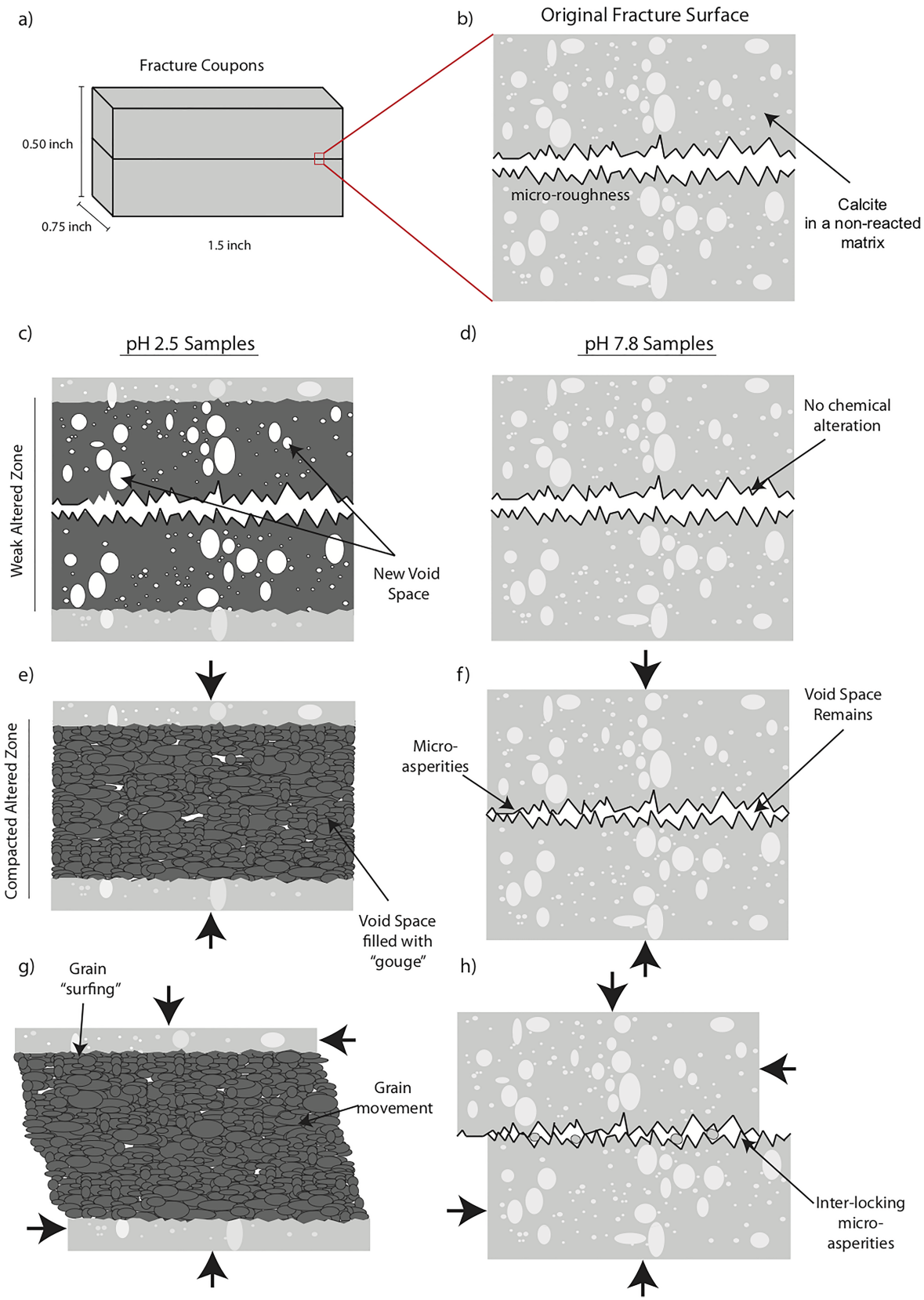

Figure 8. Schematic conceptualization of the (a) the fracture coupons and (b) their original fracture surfaces, and their configuration for the two experiments (c and d) after flow, (e and f) after initial compression, and (g and h) during shear.

4. Implications

This study presents novel experiments that exposed rock fractures to reactive flow and then compressed and sheared them. The experiments demonstrated how reaction with acidic brine can alter fracture surfaces and affect fracture fluid flow and frictional properties. The results show that acidic brine flow in a carbonate-rich shale preferentially dissolved calcite grains and created a porous layer at the fracture surface. This layer collapsed under normal stress into a fine layer of particles that impeded flow. This collapse resulted in permeability measurements 1 to 2 orders of magnitude lower than samples exposed to neutral brine. The reduced permeability persisted during shear. In addition, this dissolution-induced collapsed layer separated the two fracture walls and prevented the formation of interlocking asperities along the fracture surface. This resulted in a decrease in frictional strength.

The results of this laboratory-scale study are relevant for constant stress boundary conditions present at the field scale in the subsurface, especially for rock fractures present in rock with heterogeneous mineralogy exposed to acid perturbations. The presence of both soluble and less-soluble minerals, such as carbonates and silicates, respectively, is necessary for fracture surfaces to develop altered porous layers that are susceptible to collapse. Experimentation with other rock samples will need to be done to determine whether the results in this study are specific to one type of mineralogy, texture, and dissolution pattern, as other studies have found dissolution to result in asperities that do not collapse under stress (Ajo-Franklin et al., 2018). In addition, constant stress boundary conditions are also required to provide the confining stresses necessary to collapse the altered layer. In nature, a combination of normal and shear stresses may be acting simultaneously, which could alter the timing or set of observations seen in this study. It should be noted that this study focuses on mineral dissolution over short time frames under consistent low pH conditions. However, longer time frames with variation in fluid chemistry could result in mineral precipitation (Kanakiya et al., 2017) and this could lead to different outcomes in fracture strength and permeability.

For evaluating risk of subsurface energy applications (Deng et al., 2017), this study has two implications. The decrease in frictional strength due to reactive flow suggests that the resulting altered layer could increase the risk of a slip event occurring. If the goal is to avoid induced slip events, this is an undesirable result. Yet reacted samples remain in the velocity-strengthening regime, suggesting that any slip events should remain aseismic. However, this study also shows that reactive flow, which has been regarded as a process that may enhance leakage (Fitts & Peters, 2013), could reduce leakage once coupled with geomechanical normal stress. For the goal of avoiding leakage, this may be a desirable result. Notably, this study further implies that coupled geochemical and geomechanical processes, not merely each process in isolation, can have a strong influence on the seismicity and leakage risks for many subsurface engineering activities that introduce mechanical and chemical perturbations in the subsurface.

Acknowledgments
This study was supported by the Department of Energy under grant DE-FE0023354 to Princeton University (via Penn State University), National Science Foundation-MRSEC program through the IAC shared facility of the Princeton Center for Complex Materials (DMR-1420541), and National Science Foundation-MRI award CBET-153871. The X-ray computed tomography (XCT) data are available at http://arks.princeton.edu/ark:/88435/dsp013f4628214.

References

Ajo-Franklin, J., Voltolini, M., Mollins, S., & Yang, L. (2018). Coupled processes in a fractured reactive system. In S. Vialle, J. Ajo-Franklin, & J. W. Carey (Eds.), *Geological Carbon Storage: Subsurface Seals and Caprock Integrity* (pp. 187–206). Book Editors: American Geophysical Union. https://doi.org/10.1002/9781119118657

Akrad, O., Miskimins, J., Prasad, M. (2011) The effects of fracturing fluid on shale rock mechanical properties and proppant embedment. *Society of Petroleum Engineers Annual Technical Conference,* SPE 146658.

Benson, S. M., & Cole, D. R. (2008). CO_2 sequestration in deep sedimentary formations. *Elements*, *4*(5), 325–331.

Bielicki, J. M., Langenfeld, J. K., Tao, Z., Middleton, R. S., Menefee, A. H., & Clarens, A. F. (2018). The geospatial and economic viability of CO_2 storage in hydrocarbon depleted fractured shale formations. *International Journal of Greenhouse Gas Control*, *75*, 2–23.

Borgia, A., Pruess, K., Kneafsey, T. J., Oldenburg, C. M., & Pan, L. (2012). Numerical simulation of salt precipitation in the fractures of a CO_2-enhanced geothermal system. *Geothermics*, *44*, 13–22. https://doi.org/10.1016/j.geothermics.2012.06.002

Bourg, I. C. (2015). Sealing shales versus brittle shales: A sharp threshold in the material properties and energy technology uses of fine-grained sedimentary rocks. *Environmental Science & Technology Letters*, *2*(10), 255–259. https://doi.org/10.1021/acs.estlett.5b00233

Cornet, F. H., Helm, J., Poitrenaud, H., & Etchecopar, A. (1997). Seismic and aseismic slips induced by large-scale fluid injections. *Pure and Applied Geophysics*, *150*(3-4), 563–583.

Dávila, G., Luquot, L., Soler, J. M., & Cama, J. (2016). Interaction between a fractured marl caprock and CO_2-rich sulfate solution under supercritical CO_2 conditions. *International Journal of Greenhouse Gas Control*, *48*, 105–119. https://doi.org/10.1016/j.ijggc.2015.11.005

Deng, H., Bielicki, J. M., Oppenheimer, M., Fitts, J. P., & Peters, C. A. (2017). Leakage risks of geologic CO_2 storage and the impacts on the global energy system and climate change mitigation. *Climatic Change*, *144*(2), 151–163. https://doi.org/10.1007/s10584-017-2035-8

Deng, H., Ellis, B. R., Peters, C. A., Fitts, J. P., Crandall, D., & Bromhal, G. S. (2013). Modifications of carbonate fracture hydrodynamic properties by CO_2-acidified brine flow. *Energy and Fuels*, *27*(8), 4221–4231. https://doi.org/10.1021/ef302041s

Deng, H., Fitts, J. P., Crandall, D., McIntyre, D., & Peters, C. A. (2015). Alterations of fractures in carbonate rocks by CO_2-acidified brines. *Environmental Science and Technology*, *49*(16), 10,226–10,234. https://doi.org/10.1021/acs.est.5b01980

Deng, H., Molins, S., Steefel, C., DePaolo, D., Voltolini, M., Yang, L., & Ajo Franklin, J. (2016). A 2.5D reactive transport model for fracture alteration simulation. *Environmental Science and Technology*, *50*(14), 7564–7571. https://doi.org/10.1021/acs.est.6b02184

Deng, H., & Peters, C. A. (2019). Reactive transport simulation of fracture channelization and transmissivity evolution. *Environmental Engineering Science*, *36*(1), 90–101. https://doi.org/10.1089/ees.2018.0244

Deng, H., Steefel, C., Molins, S., & DePaolo, D. (2018). Fracture evolution in multimineral systems: The role of mineral composition, flow rate, and fracture aperture heterogeneity. *ACS Earth and Space Chemistry*, *2*(2), 112–124. https://doi.org/10.1021/acsearthspacechem.7b00130

Deng, H., Voltolini, M., Molins, S., Steefel, C., DePaolo, D., Ajo-Franklin, J., & Yang, L. (2017). Alteration and erosion of rock matrix bordering a carbonate-rich shale fracture. *Environmental Science and Technology*, *51*(15), 8861–8868. https://doi.org/10.1021/acs.est.7b02063

Dieterich, J. H. (1978). Time-dependent friction and the mechanics of stick-slip. *Pure and Applied Geophysics*, *116*(4-5), 790–806. https://doi.org/10.1007/BF00876539

Dieterich, J. H. (1979). Modeling of rock friction 1. experimental results and constitutive equations. *Journal of Geophysical Research: Solid Earth*, *84*(B5), 2161–2168. https://doi.org/10.1029/JB084iB05p02161

Elkhoury, J. E., Ameli, P., & Detwiler, R. L. (2013). Dissolution and deformation in fractured carbonates caused by flow of CO_2 rich brine under reservoir conditions. *International Journal of Greenhouse Gas Control*, *16*, S203–S215. https://doi.org/10.1016/j.ijggc.2013.02.023

Ellis, B., Peters, C., Fitts, J., Bromhal, G., McIntyre, D., Warzinski, R., & Rosenbaum, E. (2011). Deterioration of a fractured carbonate caprock exposed to CO_2-acidified brine flow. *Greenhouse Gases: Science and Technology*, *1*(3), 248–260. https://doi.org/10.1002/ghg.25

Ellis, B. R., Crandell, L. E., & Peters, C. A. (2010). Limitations for brine acidification due to SO_2 co-injection in geologic carbon sequestration. *International Journal of Greenhouse Gas Control*, *4*(3), 575–582. https://doi.org/10.1016/j.ijggc.2009.11.006

Ellis, B. R., & Peters, C. A. (2016). 3D mapping of calcite and a demonstration of its relevance to permeability evolution in reactive fractures. *Advances in Water Resources*, *95*, 246–253. https://doi.org/10.1016/j.advwatres.2015.07.023

Ellsworth, W. L. (2013). Injection-induced earthquakes. *Science*, *341*(6142), 1225942. https://doi.org/10.1126/science.1225942

Fang, Y., den Hartog, S. A. M., Elsworth, D., Marone, C., & Cladouhos, T. (2016). Anomalous distribution of microearthquakes in the Newberry Geothermal Reservoir: Mechanisms and implications. *Geothermics*, *63*, 62–73. https://doi.org/10.1016/j.geothermics.2015.04.005

Fang, Y., Elsworth, D., Ishibashi, T., & Zhang, F. (2018). Permeability evolution and frictional stability of fabricated fractures with specified roughness. *Journal of Geophysical Research: Solid Earth*, *123*, 9355–9375. https://doi.org/10.1029/2018JB016215

Fang, Y., Elsworth, D., Wang, C., Ishibashi, T., & Fitts, J. P. (2017). Frictional stability-permeability relationships for fractures in shales. *Journal of Geophysical Research: Solid Earth*, *122*, 1760–1776. https://doi.org/10.1002/2016JB013435

Fang, Y., Elsworth, D., Wang, C., & Jia, Y. (2018). Mineralogical controls on frictional properties and shear permeability evolution of fractures. *Journal of Geophysical Research: Solid Earth*, *123*, 3549–3563. https://doi.org/10.1029/2017JB015338

Faoro, I., Niemeijer, A., Marone, C. C., & Elsworth, D. (2009). Influence of shear and deviatoric stress on the evolution of permeability in a fractured rock. *Journal of Geophysical Research*, *114*. https://doi.org/10.1029/2007JB005372

Fitts, J. P., & Peters, C. A. (2013). Caprock fracture dissolution and CO_2 leakage. *Reviews in Mineralogy and Geochemistry*, *77*(1), 459–479. https://doi.org/10.2138/rmg.2013.77.13

Gaus, I. (2010). Role and impact of CO_2-rock interactions during CO_2 storage in sedimentary rocks. *International Journal of Greenhouse Gas Control*, *4*(1), 73–89. https://doi.org/10.1016/j.ijggc.2009.09.015

Guglielmi, Y., Cappa, F., Avouac, J.-P., Henry, P., & Elsworth, D. (2015). Seismicity triggered by fluid injection-induced aseismic slip. *Science*, *348*(6240), 1224–1226. https://doi.org/10.1126/science.aab0476

Hawkes, C. D., Mclellan, P. J., & Bachu, S. (2005). Geomechanical factors affecting geological storage of CO_2 in depleted oil and gas reservoirs. *Journal of Canadian Petroleum Technology*, *44*(10), 52–61.

Heiduc, W. K., & Wong, S.-W. (1996). Hydration swelling of water-absorbing rocks: A constitutive model. *International Journal for Numerical and Analytical Methods in Geomechanics*, *20*(6), 403–430. https://doi.org/10.1002/(SICI)1096-9853(199606)20:6<403::AID-NAG832>3.0.CO;2-7

Ikari, M. J., Marone, C., & Saffer, D. M. (2011). On the relation between fault strength and frictional stability. *Geology*, *39*(1), 83–86. https://doi.org/10.1130/G31416.1

Ikari, M. J., Saffer, D. M., & Marone, C. (2009). Frictional and hydrologic properties of clay-rich fault gouge. *Journal of Geophysical Research*, *114*, B05409. https://doi.org/10.1029/2008JB006089

Ishibashi, T., Elsworth, D., Fang, Y., Riviere, J., Madara, B., & Asanuma, H. (2018). Friction-stability-permeability evolution of a fracture in granite. *Water Resources Research*, *54*, 9901–9918. https://doi.org/10.1029/2018WR022598

Kanakiya, S., Adam, L., Esteban, L., Rowe, M. C., & Shane, P. (2017). Dissolution and secondary mineral precipitation in basalts due to reactions with carbonic acid. *Journal of Geophysical Research: Solid Earth*, *122*, 4312–4327. https://doi.org/10.1002/2017JB014019

Kohli, A. H., & Zoback, M. D. (2013). Frictional properties of shale reservoir rocks. *Journal of Geophysical Research: Solid Earth*, *118*, 5109–5125. https://doi.org/10.1002/jgrb.50346

Majer, E. L., Baria, R., Stark, M., Oates, S., Bommer, J., Smith, B., & Asanuma, H. (2007). Induced seismicity associated with Enhanced Geothermal Systems. *Geothermics*, *36*(3), 185–222. https://doi.org/10.1016/j.geothermics.2007.03.003

Marone, C. (1997). On the rate of frictional healing and the constitutive law for time- and slip-dependent friction. *International Journal of Rock Mechanics and Mining Sciences & Geomechanics Abstracts*, *34*(3–4), 347. https://doi.org/10.1016/S1365-1609(97)00054-3

Moeck, I., Kwiatek, G., & Zimmermann, G. (2009). Slip tendency analysis, fault reactivation potential and induced seismicity in a deep geothermal reservoir. *Journal of Structural Geology*, *31*(10), 1174–1182. https://doi.org/10.1016/j.jsg.2009.06.012

Niemeijer, A. R., & Collettini, C. (2013). Frictional properties of a low-angle normal fault under in situ conditions: Thermally-activated velocity weakening. *Pure and Applied Geophysics*, *171*(10), 2641–2664.

Niemeijer, A. R., & Spiers, C. J. (2007). A microphysical model for strong velocity weakening in phyllosilicate-bearing fault gouges. *Journal of Geophysical Research*, *112*, B10405. https://doi.org/10.1029/2008JB006089

Noiriel, C., Madé, B., & Gouze, P. (2007). Impact of coating development on the hydraulic and transport properties in argillaceous limestone fracture. *Water Resources Research*, *43*, W09406. https://doi.org/10.1029/2006WR005379

Norrish, K., & Quirk, J. P. (1954). Crystalline swelling of montmorillonite: Use of electrolytes to control swelling. *Nature*, *173*(4397), 255–256. https://doi.org/10.1038/173255a0

Pearce, J. K., & Dawson, G. K. W. (2018). Experimental determination of impure CO_2 alteration of calcite cemented cap-rock, and long term predictions of cap-rock reactivity. *Geosciences*, *8*(7), 241. https://doi.org/10.3390/geosciences8070241

Pluymakers, A. M. H., Samuelson, J. E., Niemeijer, A. R., & Spiers, C. J. (2014). Effects of temperature and CO_2 on the frictional behavior of simulated anhydrite fault rock. *Journal of Geophysical Research: Solid Earth*, *119*, 8728–8747. https://doi.org/10.1002/2014JB011575

Polak, A., Elsworth, D., Liu, J., & Grader, A. S. (2004). Spontaneous switching of permeability changes in a limestone fracture with net dissolution. *Water Resources Research*, *40*(3), W035021–W0350210. https://doi.org/10.1029/2003WR002717

Rinaldi, A. P., Vilarrasa, V., Rutqvist, J., & Cappa, F. (2015). Fault reactivation during CO_2 sequestration: Effects of well orientation on seismicity and leakage. *Greenhouse Gases: Science and Technology*, *5*(5), 645–656. https://doi.org/10.1002/ghg.1511

Rohmer, J., Pluymakers, A., & Renard, F. (2016). Mechano-chemical interactions in sedimentary rocks in the context of CO_2 storage: Weak acid, weak effects? *Earth-Science Reviews*, *157*, 86–110. https://doi.org/10.1016/j.earscirev.2016.03.009

Rohmer, J., Tremosa, J., Marty, N. C. M., & Audigane, P. (2017). Modelling of the CO_2-induced degradation of a fractured caprock during leakage: Potential for a mechanical self-limiting process. *Rock Mechanics and Rock Engineering*, *50*(10), 2763–2783. https://doi.org/10.1007/s00603-017-1260-9

Ruina, A. (1983). Slip instability and state variable friction laws. *Journal of Geophysical Research*, *88*(B12), 10,359–10,370. https://doi.org/10.1029/JB088iB12p10359

Samuelson, J., & Spiers, C. J. (2012). Fault friction and slip stability not affected by Co2 storage: Evidence from short-term laboratory experiments on north sea reservoir sandstones and caprocks. *International Journal of Greenhouse Gas Control*, *11*(SUPPL), 78–90. https://doi.org/10.1016/j.ijggc.2012.09.018

Segall, P., & Fitzgerald, S. D. (1998). A note on induced stress changes in hydrocarbon and geothermal reservoirs. *Tectonophysics*, *289*(1-3), 117–128. https://doi.org/10.1016/S0040-1951(97)00311-9

Scholz, C. H. (1998). Earthquakes and friction laws. *Nature*, *391*(6662), 37–42. https://doi.org/10.1038/34097

Spokas, K., Peters, C. A., & Pyrak-Nolte, L. (2018). Influence of rock mineralogy on reactive fracture evolution in carbonate-rich caprocks. *Environmental Science & Technology*, *52*(17), 10,144–10,152. https://doi.org/10.1021/acs.est.8b01021

Talwani, P. (1997). On the nature of reservoir-induced seismicity. *Pure and Applied Geophysics*, *150*(3-4), 473–492. https://doi.org/10.1007/s000240050089

Walsh, F. R. III, & Zoback, M. D. (2016). Probabilistic assessment of potential fault slip related to injection induced earthquakes: Application to north-central Oklahoma, USA. *Geology*, *44*(12), 991–994. https://doi.org/10.1130/G38275.1

Wang, C., Elsworth, D., & Fang, Y. (2017). Influence of weakening minerals on ensemble strength and slip stability of faults. *Journal of Geophysical Research: Solid Earth*, *122*, 7090–7110. https://doi.org/10.1002/2016JB013687

Wilkins, R., Menefee, A. H., & Clarens, A. F. (2016). Environmental life cycle analysis of water and CO_2-based fracturing fluids used in unconventional gas production. *Environmental Science and Technology*, *50*(23), 131–134.

Witherspoon, P. A., Wang, J. S. Y., Iwai, K., & Gale, J. E. (1980). Validity of cubic law for fluid flow in a deformable rock fracture. *Water Resources Research*, *16*(6), 1016–1024. https://doi.org/10.1029/WR016i006p01016

Xu, T., & Pruess, K. (2004). Numerical simulation of injectivity effects of mineral scaling and clay swelling in a fractured geothermal reservoir. *Transactions - Geothermal Resources Council*, *28*, 269–278.

Zoback, M. D., & Gorelick, S. M. (2012). Earthquake triggering and large-scale geologic storage of carbon dioxide. *Proceedings of the National Academy of Sciences of the United States of America*, *109*(26), 10,164–10,168. https://doi.org/10.1073/pnas.1202473109